Journal of Porous Materials (2020) 27:1589–1599
https://doi.org/10.1007/s10934-020-00937-6

Preparation of nanofiber aerogels by electrospinning and studying of its adsorption properties for heavy-metal and dyes

Longqi Xue[1] · Jing Ren[1,2] · Shugang Wang[1] · Dehui Qu[1,2] · Zhonglin Wei[1] · Qingbiao Yang[1,3,4] · Yaoxian Li[1]

Published online: 14 July 2020

Abstract

Developing novel and efficient adsorption materials to solve water pollution is a very challenging task for the sake of environmental protection and human health. Herein, an ultra-light and porous 3D nanofiber aerogels (NFA) has been prepared by freezing casting technology and cross-linking with epichlorohydrin(ECH) via short polyacrylonitrile (PAN)/polyetherimide (PEI) nanofibers, which features high mechanical stability and good mass transfer performance. Moreover, experiments show that the adsorption capacities of 3D nanofiber aerogels (NFA) for Cu(II), Cr(VI), As(V) and anionic dye methyl orange (MO) reach 242.71 mg/g, 214.14 mg/g, 258.36 mg/g and 183.06 mg/g, respectively. Importantly, the adsorbent still maintains considerable adsorption efficiency after seven adsorption-regeneration cycles.

Keywords Electrospinning · Adsorption · Nanofiber aerogels (NFA) · Regeneration

1 Introduction

With the development of industry, heavy metal ions and dyes from chemical, metallurgical and dyeing industries have become major causes of water pollution [1]. Among the heavy metal ions and dyes, one of the most widely distributed heavy metals is copper. Copper and its alloys are widely used in the metallurgical industry and electrical industry. Excessive copper exposure or consumption may cause brain, liver, respiratory and nervous system diseases, especially in children. Therefore, copper has been listed as a priority pollutant by the US Environmental Protection Agency, and the presence and removal of residual copper ions in water must be checked [2]. Chromium is widely used in metal processing, electroplating and leather industries. A large amount of Cr (VI) ions may penetrate into the surface soil through industrial discharge, causing pollution of groundwater, rivers and lakes, accumulating in the human body through the food chain and inducing cancer. Therefore, the government lists hexavalent chromium as a priority pollutant, and the removal of hexavalent chromium is of great significance [3, 4]. In recent years, arsenic in water and food has been reported to cause nerve, cardiovascular, respiratory and liver damage as well as skin cancer, bladder cancer and lung cancer. Therefore, the existence of arsenic in natural water is a global problem, and the removal of arsenic is crucial [5]. In addition, as another major source of water pollution, organic dyes are not easily degraded and are harmful to many organisms. Therefore, the removal of organic dyes pollutants in wastewater has always been the focus of research [6]. People are paying more and more attention to the serious threat to people's lives and health [7–9]. Now, the removal of these heavy metal ions and dyes from wastewater by adsorption, ion exchange, separation and precipitation

Longqi Xue and Jing Ren contributed equally to this article.

Electronic supplementary material The online version of this article (https://doi.org/10.1007/s10934-020-00937-6) contains supplementary material, which is available to authorized users.

✉ Qingbiao Yang
yangqb@jlu.edu.cn

1 College of Chemistry, Jilin University, Changchun 130021, People's Republic of China

2 College of Materials Science and Engineering, Jilin University of Chemical Technology, Jilin 132022, People's Republic of China

3 Jilin Provincial Key Laboratory of Lymphatic Surgery, China-Japan Union Hospital of Jilin University, Changchun 130031, People's Republic of China

4 College of Chemistry, Jilin University, Changchun 130061, People's Republic of China

has attracted many researchers' attention. Among them, the adsorption method after the introduction of nanotechnology and nanostructured materials is one of the most promising separation methods to remove metal ions and dyes due to its high efficiency and environmental friendliness [10–12]. Traditional nanostructured adsorbents include nanobeads [13], nanocomposites [14], magnetic nanosorbents [15] and electrospun nanofiber members [16–19]. Among them, the electrospun nanofiber membranes adsorbent has been widely used in water treatment due to its large specific surface area, high adsorption efficiency, recovery and regeneration after completion of adsorption. In recent years, a new type of 3D nanofiber aerogel constructed from short nanofibers has attracted growing interests for widespread applications due to their fantastic properties. In 2014, density-tunable, porous, 3D elastic nanofiber aerogels were first constructed by Ding's team from short nanofibers [20]. 3D electrospun nanofiber aerogels have been widely used in supercapacitors electrodes [21–24], sound insulation [25], thermal insulation [26], pressure sensing [27], oil–water separation [28, 29], catalysis [30], drug carriers [31] and adsorption [32–34] due to its low density, high hole, favorable structural stability. However, few applications have been reported on the adsorption of heavy metal ions and dyes. In 2015, Canhui Lu team synthesized a new dendrimer poly (amidoamine) grafted cellulose nanofiber (PAMAM-g-CNF) aerogels for Cr (VI) removal [32]. In 2018, the Sara Mousavi team used a freeze casting process and then thermal cross-linking to synthesize an ultra-light and robust pullulan/polyvinyl alcohol/polyacrylic acid 3D nanofiber aerogels (NFA) with adjustable porosity and flexibility. Its ability to adsorb cationic dyes and its reusability were investigated [34]. The construction of 3D nanofibers with porous networks greatly enriches the potential adsorption sites inside the nanofibers, and the high porosity and interconnected porous structure promote the diffusion and transport of molecules. Thus, the defects of the metal ions from the nanofiber surface to the interior are overcome. Besides, 3D nanofiber structure adsorbent has better structural stability than nanofiber membrane adsorbent. Up to now, as far as we known, the adsorption of anionic dyes and heavy metal such as Cu (II) and As (V) ions by this 3D nanofiber aerogels structure has not been reported.

In addition, Polyethyleneimine (PEI) contains numerous cationic amine groups on its linear macromolecular chains, which have a very high affinity to metal ions and anionic dyes [35, 36]. It is a novel polyamine-type heavy metal ion trapping agent and often used as a precipitant in water treatment, but sludge is produced, causing secondary pollution [37, 38]. PEI is easily soluble in water with poor mechanical properties which limit its practical application. So it is greatly significant how to obtain PEI solid materials that are insoluble in water, in this study the water-soluble polyethylenimine (PEI) could be cross-linked by using the epichlorohydrin (ECH), which provides the PEI with good water resistance [39–41]. Therefore, we obtained the 3D nanofiber aerogels (NFA) with PAN as the backbone, PEI as the metal ions and anionic dyes trapping agent and ECH as the cross-linker, and studied its adsorption properties for heavy metal ions and organic dyes. We found that it has good adsorption properties compared to similar adsorbents (Online Resource 1 Table S1).

2 Materials and methods

2.1 Chemicals

Polyacrylonitrile (PAN) fiber was provided by Jilin Petrochemical Company; Polyethylenimine (PEI) was obtained from GongBike New Material Technology Co., Ltd. Epichlorohydrin (ECH) Aladdin reagent Shanghai Co., Ltd. Methyl Orange (MO), Potassium Bromide (KBr) were purchased from Tianjin Guangfu Fine Chemical Research; Na_3AsO_4•$12H_2O$ was provided by Hengyang Chemical Raw Material Factory; *N,N*-Dimethylformamide (DMF), Potassium dichromate,Lead nitrate, copper sulfate pentahydrate, potassium hydroxide were all purchased from Beijing Chemical Reagent Factory.

2.2 Preparation of PAN/PEI nanofibers

PAN and DMF were added into a 100 mL flask respectively, and dissolved under stirring at 45 °C to obtain a 7.0 wt.% PAN solution. After cooling to room temperature, a certain amount of PEI was added. Along with stirring for 2 h, a homogeneous transparent PAN/PEI solution was obtained. Then the PAN/PEI solution was filled into a 20 ml syringe. The electrospinning was conducted at 20 kV voltage, 1.5 mL/h flow rate and 15 cm distance between collector and a tip of the above syringe with a 0.84 mm inner diameter metal needle. Continuous spinning for 2 h at room temperature and air relative humidity of 10%, the smooth, flat, soft, fluffy PAN/PEI electrospun nanofibers were obtained.

2.3 Preparation of porous 3D PAN/PEI/ECH nanofiber aerogels (NFA)

The above PAN/PEI electrospun nanofibers (1.0 g) were cut into small square pieces with a side length of 0.5 cm and immersed in 50 g distilled water. The mixture was homogenized at 14,000 rpm for 20 min using a T-25 homogenizer (IKA, German). We investigated the freezing time and the freezing temperature to study its freezing effect (Online Resource 1 Figure S1). The obtained dispersed short nanofibers were fixed by freezing at -60 °C for 30 min. At the same time, the solvent between the dispersions crystallized.

The sample was then placed in a freeze dryer and freeze-dried at – 50 °C for 48 h to obtain PAN/PEI porous material. Next, considering PEI is a water-soluble polymer, it needs to be treated as an insoluble substance. Since PEI contains lots of highly active amine groups, cross-linked 3D PAN/PEI/ECH NFA can be obtained after cross-linking with epichlorohydrin (ECH). In this work, for the preparation of PAN / PEI crosslinking by ECH, first place the freeze-dried PAN / PEI aerogel in 50 ml acetone: ECH (4: 1, v: v), crosslink for 10 h at room temperature, Wash with ethanol, deionized water in sequence, and then freeze-dry to obtain cross-linked PAN / PEI / ECH nanofiber aerogel. The specific preparation process is shown as Fig. 1.

2.4 Batch Adsorption experiment

Aqueous solutions of different concentrations of Cu(II), Cr(VI), As(V), Methyl Orange (MO), were prepared. Take 20 ml of the above solutions respectively and transfer them to the corresponding 50 ml Erlenmeyer flask. Porous PAN/PEI/ECH NFA was cut into fragments of the same mass. Each portion was added to the above Erlenmeyer flask at 25 °C, respectively. The PAN/PEI/ECH NFA were removed after the adsorption experiment lasted for several hours. The concentration of the solution before and after adsorption was measured by ICP and UV spectroscopy, and the equilibrium adsorption capacity q_e was calculated according to formula (1) [34]:

$$q_e = \frac{(c_o - c_e)v}{m} \quad (1)$$

where: C_0 and C_e are the concentration of the solution before and after adsorption (mg/L); V are the volume of the solution (L); m is the mass of the porous PAN/PEI/ECH NFA (g).

3 Results and discussion

3.1 Characterization

3.1.1 Morphology characterization of 3D porous PAN/PEI/ECH NFA

The SEM image exhibits the hierarchical pore architecture of the aerogels material, as shown in Fig. 2a, nanofibers are stacked before cross-linking. These aerogels absorb water very easily, shrink and deform, and are difficult to recycle. After cross-linking with ECH, Fig. 2b shows that the diameter of the PAN / PEI fibers becomes significantly larger, and it can be clearly observed that NFA has a rich cross-linking network structure. The three-dimensional network structure makes the holes become more solid, and the resilience of the material also becomes stronger.

3.1.2 Infrared spectrum analysis

The chemical structures of PAN/PEI fibers before and after cross-linking with ECH were determined by FTIR spectroscopy. Figure 3 shows that the position of the –CN characteristic absorption peak at 2236 cm^{-1} did not change after the cross-linking reaction occurred, indicating that PAN did not participate in the reaction and was only used as a template carrier. The vibration absorption peak of tertiary amine C–N bond at 1069 cm^{-1} (line b) is obviously enhanced. The N–H tensile vibration absorption peak of amine group at 3423 cm^{-1} and the deformation vibration absorption peak at 788 cm^{-1} (line b) are both weakened.

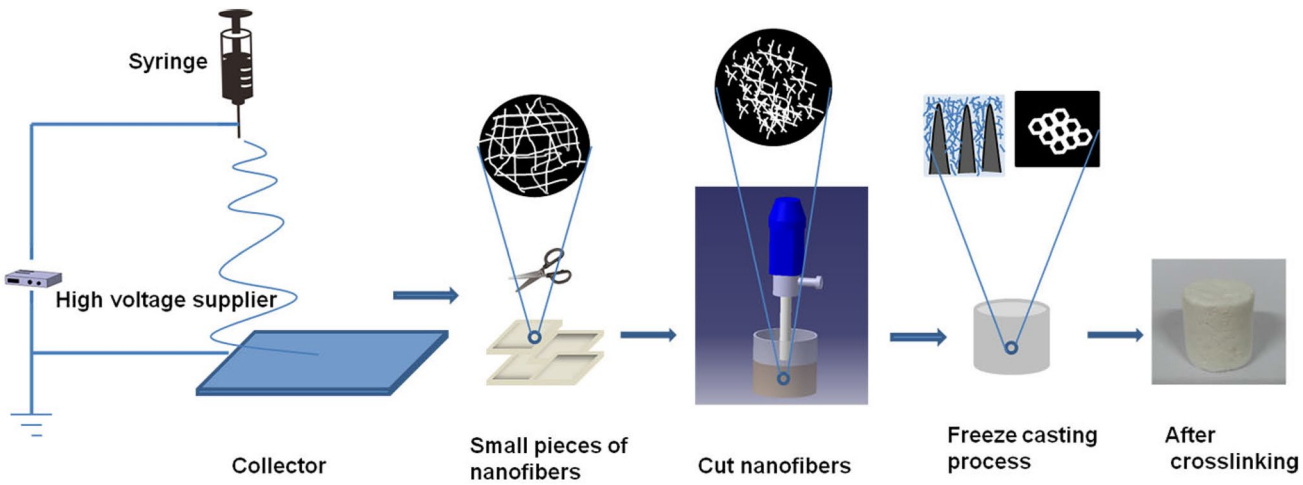

Fig. 1 The preparation process of PAN/PEI/ECH nanofiber aerogel

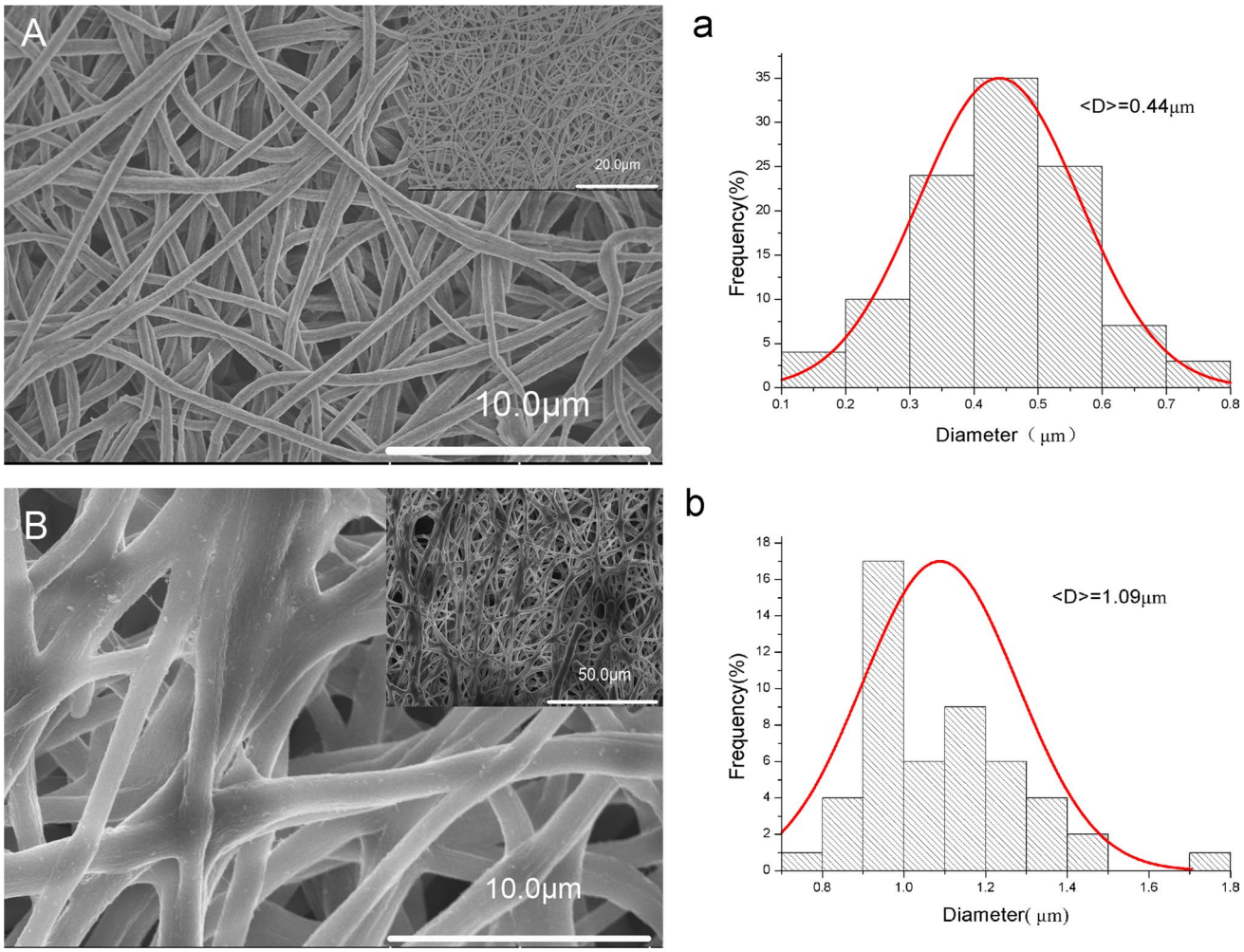

Fig. 2 The SEM images and diameters distributions of PAN/PEI NFA (A, a) (SU8000 3.0KV 8.2 mm*5.0 K SE(U)) and PAN/PEI/ECH NFA (B, b) (SU8000 10.0KV 8.2 mm*5.0 K SE(U))

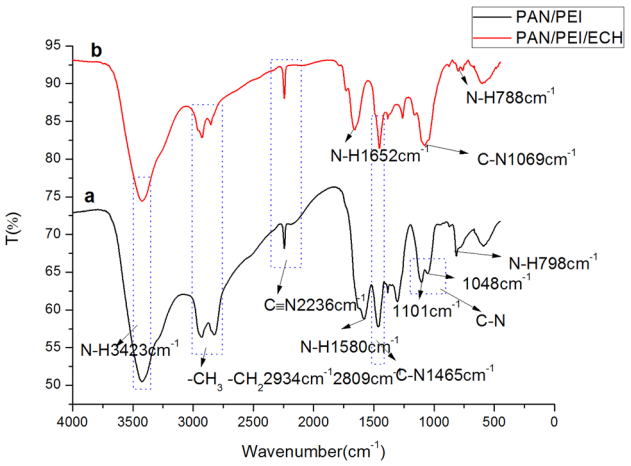

Fig. 3 The infrared spectra of PAN/PEI aerogel before (**a**) and after (**b**) cross-linking reaction

It indicates that H atoms on N–H bond of primary and secondary amine groups have been replaced by methylene group of epichlorohydrin. Through dehydrochlorination reaction and ring-opening reaction of epoxy bond, both primary and secondary amine groups have become tertiary amine groups.

3.2 Adsorption

3.2.1 Adsorption selectivity of PAN/PEI/ECH NFA for dyes

In order to investigate the adsorption properties of PAN/PEI/ECH aerogels on dyes, we selected seven different types of organic dyes for adsorption selectivity experiments. We found that NFA has a good adsorption effect on anionic dyes.(Online Resource 1 Fig. S2).

3.2.2 Effect of pH, adsorbent dosage and adsorption time

The effect of pH on the Cu(II), Cr(VI), As(V) and MO adsorption performance using PAN/PEI/ECH aerogels was studied. As (Online Resource 1 Fig. S3A) depicted, the Cu(II) adsorption capacity increases with increasing pH and then decreases slightly. The maximum adsorption capacity is produced at approximately pH 5.0. This is perhaps in virtue of the fact that the amine groups on the aerogels can be protonated at lower pH values, thereby inducing strong electrostatic repulsion of the metal cations [42]. In the pH range of 6.0–7.0, the metal cation can be slightly hydrolyzed, resulting in a decrease in the amount of adsorption [43]. The (Online Resource 1 Fig. S3B) shows that the Cr(VI) uptake ability of the aerogels reached a maximum at pH 2.0, and then gradually decreased as the pH value increased. The reason for this is that $HCrO_4^-$ and $Cr_2O_7^{2-}$ were the main existence status of Cr (VI) in the pH range of 2.0–6.0, electrostatic attraction is the main driving force of the adsorption process and the decreased positive charge density could lead to the decrease of the adsorption efficiency when the pH values increased. In chromate solution with a pH of 1.0, the predominant species is H_2CrO_4, which weakens the electrostatic attraction between Cr(VI) species and protonation of amino groups [40, 43]. So the adsorption performance sharply declined at pH 1.0. Similarly, the adsorption of As(V) is also related to arsenate speciation and the protonation of PEI as a function of the pH value. (Online Resource 1 Fig. S3C) When the pH value is 2.0, the As(V) species exist in the form of H_3AsO_4, which is very hard to be adsorbed. The maximum As(V) adsorption was observed at pH 3.0, and due to the higher degree of protonation of weak amine groups in NFA, it can strongly interact with As(V) ions carrying negative charges in solution. Therefore, these As (V) substances are mainly adsorbed by electrostatic attraction [44]. The result (Online Resource 1 Fig. S3D) shows that the aerogels adsorption capacity on MO decreases as the pH value of the solution increases. The aerogels surface functional groups would result in a decrease in the positive potential of the aerogels adsorbent, thereby reducing the electrostatic interactions between MO and aerogels [45]. In order to better control the experimental variables, we need to choose the appropriate pH to investigate the adsorption capacity.

Prepare 200 mg/l, 100 mg/l, 100 mg/l, 10 mg/l Cu(II), Cr(VI), As(V) and MO aqueous solutions, respectively, and take 20 ml separately into a conical flask. In addition, 10 mg of PAN/PEI/ECH aerogels were further added and adsorbed at 25 °C for 0.5 h, 1 h, 1.5 h, 2 h, 5 h, 7 h, 10 h, 15 h, 23 h, and 30 h, respectively. Online Resource 1 Fig. S4 shows the effect of time on the adsorption properties of PAN/PEI/ECH materials. As can be seen from the figure, the PAN/PEI/ECH aerogels has a fast adsorption speed and can reach equilibrium in a short time. This may be because after freeze-drying, a large number of holes inside the material increase the contact area between the fiber and the sucked material.

Adsorption experiments were performed with different doses of NFA (0.5–5 g/L). The initial concentration of Cu(II) and As(V) was 200 mg/L, and the initial concentration of Cr(VI) and MO was 100 mg/L. As shown in Online Resource 1 Fig. S5, as the number of NFA increases, the removal rate increases in the first phase and then reaches the platform. This is because as the amount of the adsorbent increases, the surface area of the adsorbent and the number of active sites increase, which increases the removal rate of metal ions. However, when the dose of Cr(VI) and MO exceeds 1.0 g/L, the NFA dose increases due to an excessive adsorption site, and the removal rate does not increase. The decrease in adsorption capacity is attributed to the unsaturated adsorption of the adsorbent during the adsorption process.

3.2.3 The effect of coexisting ions

Since real wastewater usually contains a variety of coexisting ions, this may affect the adsorption capacity of heavy metal ions. The effects of NO_3^-, SO_4^{2-} and $H_2PO_4^-$ on anion adsorption at different ionic strengths were investigated. The competitive mechanism may reduce the adsorption capacity of Cr(VI), As(V) and MO to some extent (Online Resource 1 Fig. S6). NO_3^- is a monovalent anion which can compete slightly with protonated amines with Cr(VI), As(V) and MO, while SO_4^{2-} and $H_2PO_4^-$ are polyvalent anions which can be used for Cr(VI), As(V) and MO play a more competitive role. Although the adsorption capacities of Cr(VI), As(V) and MO decrease with increasing ionic strength, the adsorption capacity is still high. Therefore, NFA can effectively remove metal ions even in the presence of a high concentration of coexisting ions.

3.2.4 Isothermal adsorption studies

As shown in Fig. 4, the isothermal adsorption curves and Langmuir linear points of PAN/PEI/ECH NFA for metal ions and MO. In the isothermal adsorption experiment,

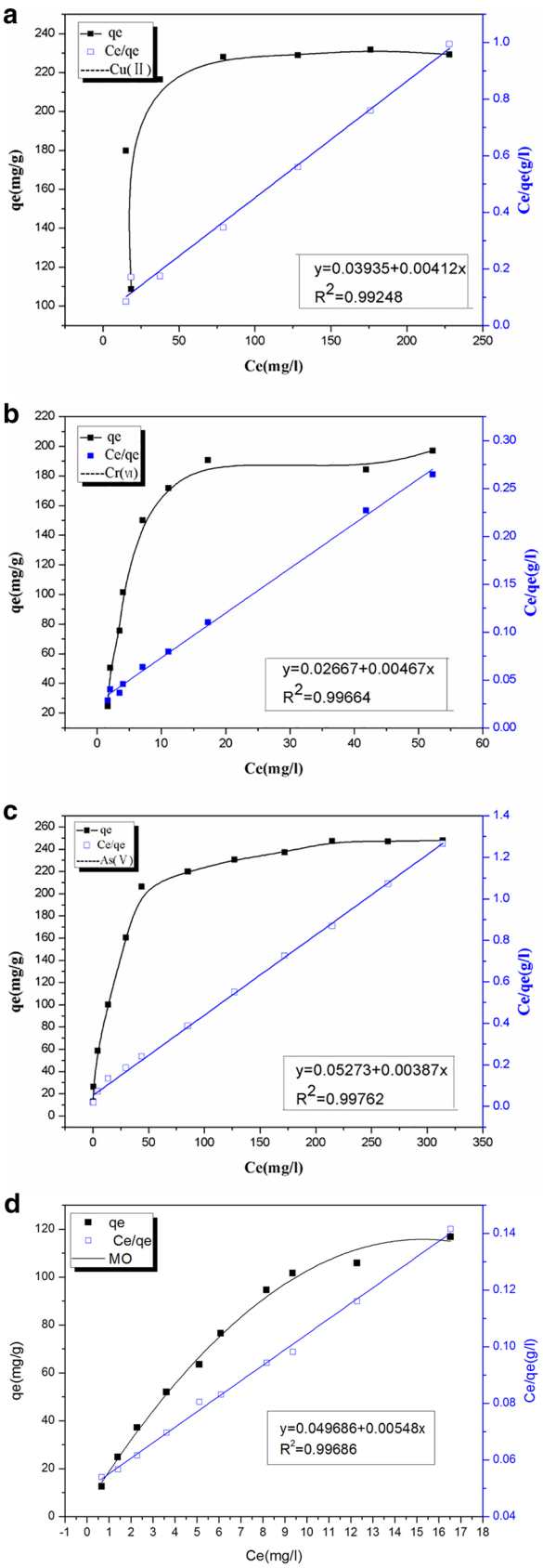

Fig. 4 Adsorption isotherm and Langmuir plot of Cu(II) (**a**), Cr(VI) (**b**) As(V) (**c**), and MO (**d**) (reaction conditions: adsorption dose 0.5 g/L, Cu(II) pH 5.0, Cr(VI) pH 2.0, As (V) pH 3.0, MO pH 6.0, adsorption time 24 h, adsorption temperature 25 °C)

we took 10 mg of adsorbent in 20 ml of different concentrations of pollutants and adsorbed at room temperature. Along with the initial concentration gradually increases, the adsorption of metal ions and dyes by the PAN/PEI/ECH NFA gradually increases, eventually reaching the adsorption equilibrium. When the initial concentration of metal ions and dyes is low, the NFA contain a large number of residual adsorption sites. With the increase of the concentration, the adsorption sites of the NFA are occupied, which leads to the retention of the adsorption capacity of the NFA when the solution reaches a certain concentration.

The quality of PAN/PEI/ECH NFA exhibits a good linear relationship to the adsorption of metal ions and MO, which is consistent with the Langmuir isothermal monolayer adsorption model. According to the formula (2) [46], the maximum adsorption amounts of Cu(II), Cr(VI), As(V), and MO for PAN/PEI/ECH NFA were 242.71 mg/g, 214.14 mg/g, 258.36 mg/g and 183.06 mg/g respectively.

$$\frac{C_e}{q_e} = \frac{1}{k_L q_{\max}} + \frac{C_e}{\max} \tag{2}$$

Among them, C_e is the equilibrium adsorption concentration (mg/L), q_e is the equilibrium adsorption capacity (mg/g), q_{max} is the maximum adsorption capacity (mg/g), and K_L is the Langmuir isothermal adsorption equilibrium constant.

3.2.5 PAN/PEI/ECH NFA kinetics study

In virtue of the pseudo-first-order kinetic equation and the pseudo-second-order kinetic equation, the adsorption behavior of PAN/PEI/ECH NFA was studied. Figure 5a–d show the adsorption behavior of PAN/PEI/ECH NFA for Cu(II), Cr(VI) and As(V) conforms to quasi-secondary adsorption kinetics and the removal of Cu(II), Cr(VI) and As(V) was a chemisorption process. On the other hand, the adsorption of MO by the PAN/PEI/ECH NFA is suitable for the pseudo-first-order kinetics model and pseudo-second-order kinetics models, and the removal of MO was a physical and chemisorption process. The linear forms of the pseudo-first-order and pseudo-second-order kinetics models can be described using the following equations [46], respectively:

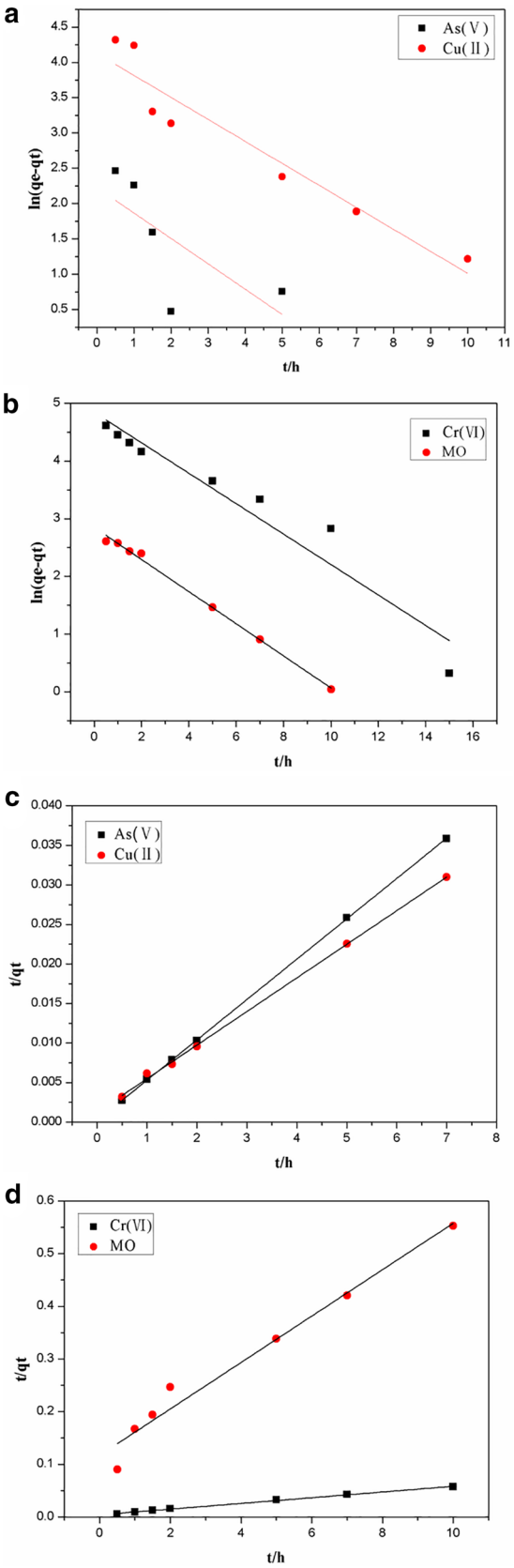

◂**Fig. 5** The Kinetic adsorption model both of pseudo-first-order (**a**) and (**b**) and pseudo -second-order (**c**) and (**d**). (reaction conditions: adsorption dose 0.5 g/L, Cu(II) pH 5.0, Cr (VI) pH 2.0, As (V) pH 3.0, MO pH 6.0, adsorption temperature 25 °C)

Table1 The kinetic adsorption model related parameters

	Pseudo-first-order		Pseudo-second-order	
	$\ln(q_e\text{-}q_t)=\ln q_e\text{-}k_1t$		$t/q_t=1/k_2q_e^2+t/q_e$	
	K_1	R_1^2	K_2	R_2^2
The kinetic adsorption model				
Cu(II)	0.45117	0.9216	0.01336	0.9997
Cr(VI)	0.2636	0.9236	0.00509	0.99665
As(V)	0.27986	0.3348	0.11985	0.99998
MO	0.2782	0.9956	0.00025	0.9668

$$\ln(q_e - q_t) = \ln q_e - k_1 t \tag{3}$$

$$\frac{t}{q_e} = \frac{1}{k_2 q_e^2} + \frac{1}{q_e} \tag{4}$$

where q_e (mg/g) and q_t (mg/g) are the sponge adsorbed at equilibrium and at time t (min), respectively; k_1 (min^{-1}) and k_2 ($g{\cdot}mg^{-1}{\cdot}min^{-1}$) are the pseudo-first-order and the pseudo-second-order rate constants of adsorption, respectively. The relevant results are shown in Table 1.

3.2.6 NFA regeneration

0.05 M NaOH was selected as desorption solution to regenerate the adsorbent. The adsorbent with methyl orange reaching saturation could be washed with ethanol. As shown in Fig. 6a, the adsorbent still maintains considerable adsorption efficiency after seven adsorption-regeneration cycles. Next, it is necessary to further evaluate the residual concentrations of these NFA after removal of cupper ions, chromate, arsenate and methyl orange. As shown in Fig. 6b when the initial concentration of the adsorbed solution is 20 mg/L, the residual concentration after NFA adsorption decreases to 0.0862 mg/L, 1.217 mg/L, 0.1873 mg/L, 0.3920 mg/L, respectively, which means about 99.6% of cupper ions, 93.9% of chromate, 99.1% arsenate and 98.0% methyl orange were removed and indicates the NFA has excellent removal ability. In particular, the content of Cu^{2+} in treated water is much lower than the WHO drinking water standard.

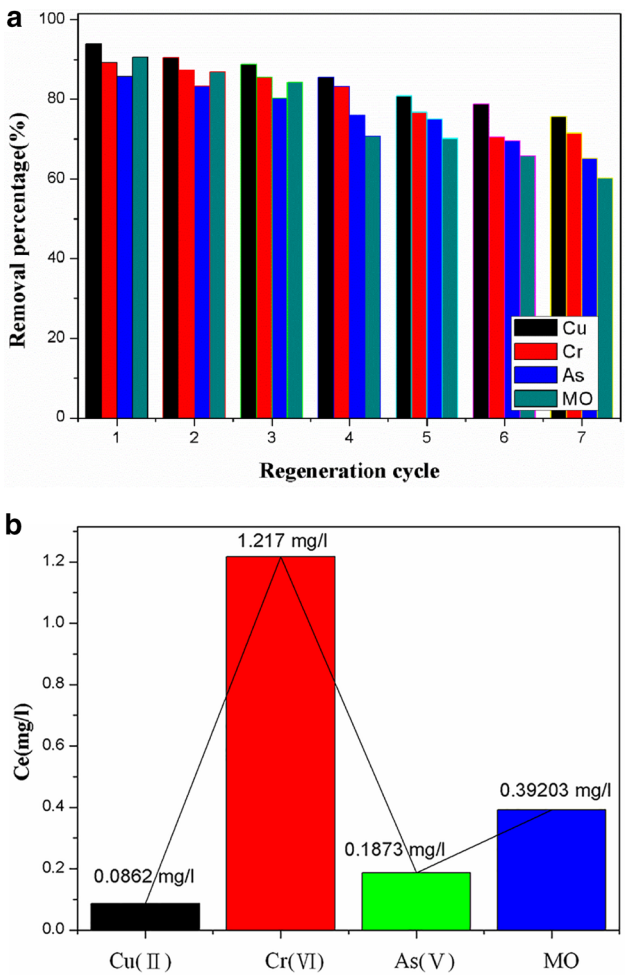

Fig. 6 The heavy metal ions and MO adsorption ability of PAN/PEI/ECH NFA at different regeneration cycles (**a**) and residual concentration (**b**) (reaction conditions: adsorption dose 5 g/L, Cu(II) pH 5.0, Cr(VI) pH 2.0, As(V) pH 3.0, MO pH 6.0, C_0 = 20 mg/L, adsorption time 24 h, adsorption temperature 25 °C)

3.2.7 XPS analysis

In order to study any possible adsorption mechanism of NFA on Cu(II), Cr(VI) and As(V), the XPS analyses of surface chemical composition before and after NFA adsorption were carried out. The Fig. 7a shows the XPS spectrum of NFA-loaded Cu(II). In compared with the XPS spectrum before NFA adsorption, the new BE signal is about at 932 eV, attributing to the Cu_{2p} species, indicating Cu(II) successfully adsorbed. The high-resolution Cu_{2p} core-level spectrum consists of Cu $2p_{3/2}$ (BE at 932.5 eV) and Cu $2p_{1/2}$ (BE at 952.9 eV) spin orbit split doublet (Fig. 7b). The high-resolution core-level spectra of N_{1s} of NFA were deconvoluted into two peaks at 398.6 and 401.3 eV, (Online Resource 1 Fig. S7A) which were assigned to the nitrogen in the neutral amines (–NH_2 or –NH–) and protonated amines (–NH_3^+ or –NH_2^+–), respectively [47]. After the NFA loaded Cu, (Online Resource 1 Fig. S7B) both of the peaks for neutral and protonated amines had shifted, suggesting that both of these two kinds of amines participating in the adsorption of copper. It can be seen from the Fig. 7a that there was a new Cr absorption peak. Interestingly, the high resolution XPS spectral Cr 2p region (Fig. 7c) indicates that the Cr $2p_{1/2}$ and Cr $2p_{3/2}$ line peaks are located at 587.4 and 578.7 to 576.4 eV. However, the two peaks of Cr $2p_{3/2}$ are designated as Cr(VI) and Cr(III) at 578.6 and 576.4 eV, respectively, indicating that Cr(VI) and Cr(III) coexist on the surface of the NFA during adsorption and part of Cr(VI) is reduced to Cr(III) [32]. The surface chemistry of NFA (before arsenic adsorption) and NFA (after arsenic adsorption) were investigated by XPS analysis. As shown in the Fig. 7a, the characteristic peak of As(V) corresponds to the binding energy of 44.0 eV [44], and it is confirmed that the arsenic ion is adsorbed on the adsorbent. From the XPS spectrum shown in the Fig. 7d, it was observed that after As(V) adsorption, this showed a broad peak with binding energy of 43.5 and 44.4 eV, which could be assigned to As(III) and As(V) [48].

3.2.8 Adsorption mechanism

Considering that NFA containing abundant amines (–NH_2), imines (–NH–) and tertiary amino groups (–N=), the lone pair of electrons of which can be donated to the empty atomic orbital Cu(II) to form amino group–metal complexes [49]. It is foreseeable that during the Cu(II) adsorption process, Cu(II) ions have a good chance to form monodentate, bidentate, tridentate and tetradentate

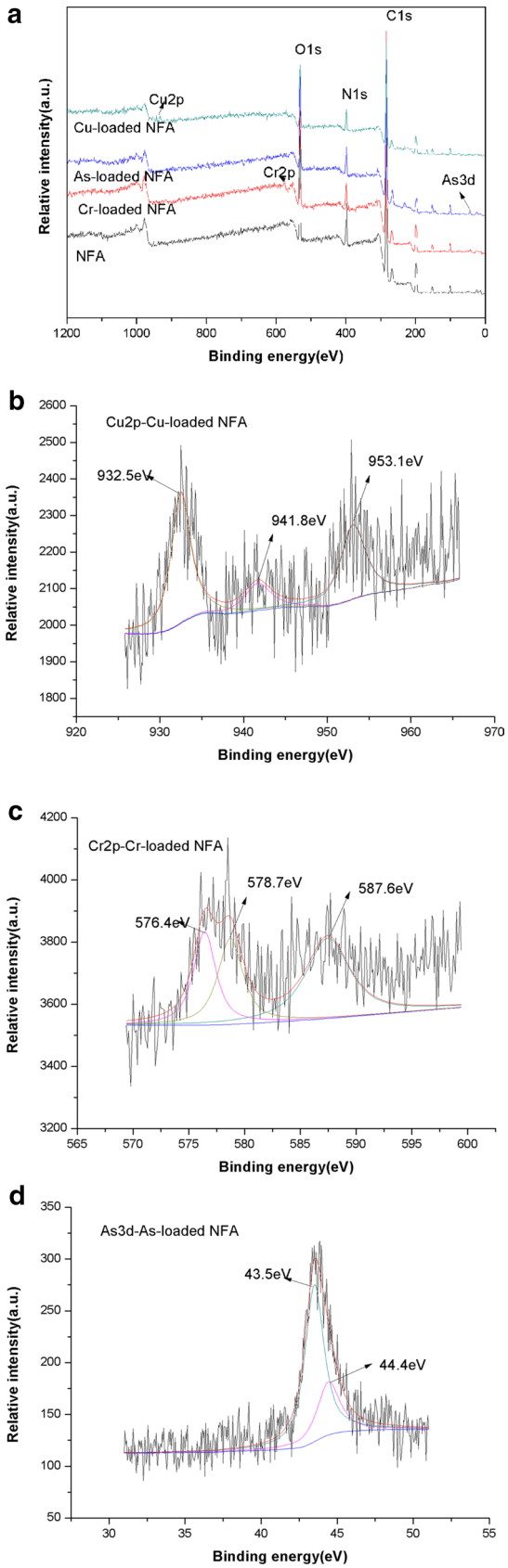

Fig. 7 **a** XPS wide scan spectrum of NFA before and after Cu(II), Cr(VI) and As(V) adsorption. The high-resolution core-level spectra of the (**b**) Cu-loaded, **c** Cr-loaded and **d** As-loaded NFA after adsorption (reaction conditions: adsorption dose 0.5 g/L, Cu(II) pH 5.0, Cr(VI) pH 2.0, As(V) pH 3.0, MO pH 6.0, $C_0 = 200$ mg/L, adsorption time 24 h, adsorption temperature 25 °C)

complexes with several NFA amino groups [50]. Therefore, we propose that the NFA form a chelate complex with Cu(II) ions to efficiently recover Cu(II) ions from aqueous solution. We propose a possible Cr(VI) removal mechanism. First, under acidic conditions, Cr(VI) ions are electrostatically attracted by amine groups protonated in NFA. Then, due to its high redox potential (above 1.3 V under standard conditions), some Cr(VI) can be easily reduced to Cr(III) by adjacent electron donor groups under acidic conditions. Finally, cation exchange can capture positively charged trivalent chromium, and the electrostatic attraction of protonated amino functional groups can capture negatively charged hexavalent chromium [3]. Similarly, protonated amine groups can strongly interact with negatively charged As(V) ions in solution. In the pH range of 2.25–11.50, two main arsenic substances ($H_2AsO_4^-$ and $HAsO_4^{2-}$) are present in the solution. Therefore, these As(V) are adsorbed as a result of electrostatic attraction [51]. In addition, the XPS spectrum of NFA after As(V) adsorption shows that a part of the adsorbed As(V) is reduced to trivalent As(III), indicating that there is a redox reaction between the adsorbent and the adsorbed oxygen anion. Similarly, the anionic organic dye (MO) is electrostatically adsorbed through protonated amino groups on NFA [52]. Mechanism is shown in Fig. 8.

4 Conclusions

A new type of 3D PAN/PEI/ECH NFA was prepared, and its adsorption properties for Cu(II), Cr(VI), As(V) and MO were studied. Due to the stable pore structure, NFA exhibits encouraging adsorption properties. The main mechanisms include the complexation reaction of NFA with Cu^{2+} and the electrostatic adsorption of Cr(VI), As(V) and MO. In addition, the pseudo-second-order kinetic model and the Langmuir adsorption isotherm model fit the reaction process well. The recoverable recycling experiment proves that NFA adsorbent has broad prospects in wastewater treatment.

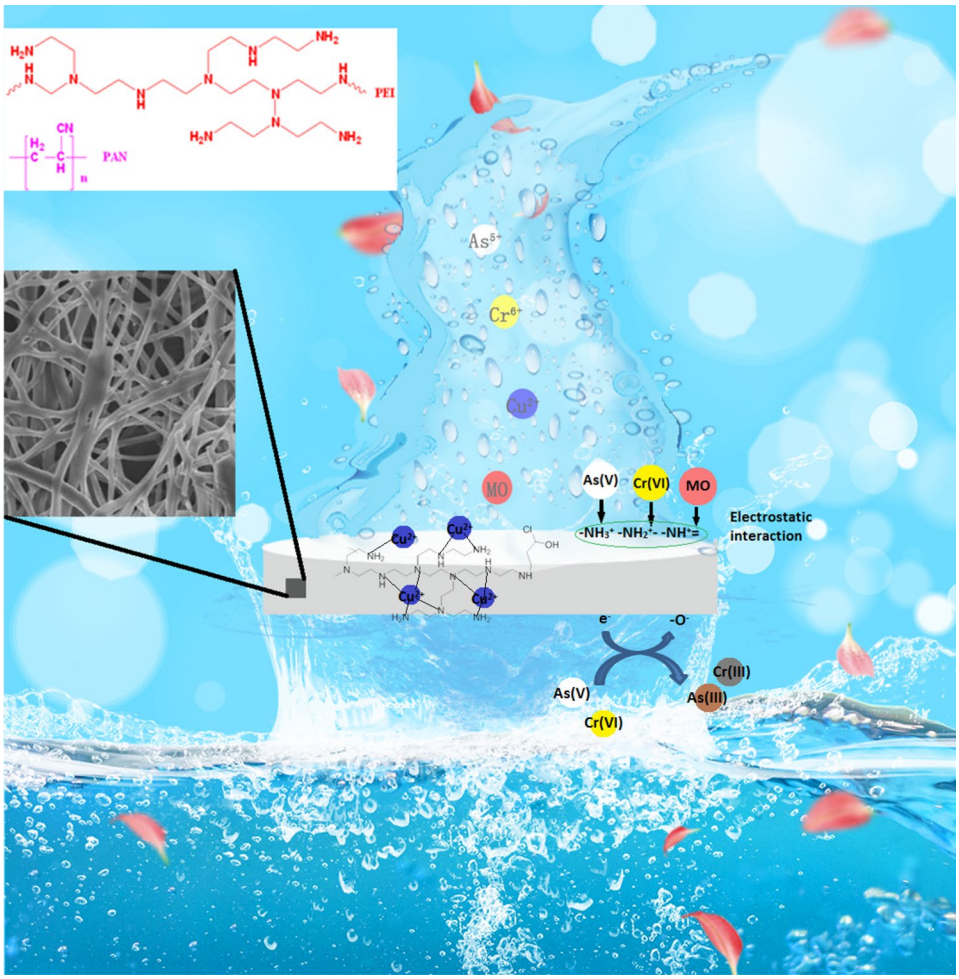

Fig. 8 The main mechanism figure of Cu(II), Cr(VI), As(V) and MO removal by NFA

Acknowledgments This study was funded by the National Natural Science Foundation of China (Contract Grant Number 21174052), Jilin Province Science and Technology Research Plan (Contract Grant Number 20180201085GX), and the Natural Science Foundation of Jilin Province of China (Contract Grant Number 20170101105JC).

Compliance with ethical standards

Conflict of interest All authors declare that they have no conflict of interest.

References

1. T. Yu, Z. Xue, X. Zhao, W. Chen, T. Mu, New J. Chem. **42**, 16154 (2018)
2. Z.A. Sutirman, E.A. Rahim, M.M. Sanagi, K.J.A. Karim, W.A.W. Ibrahim, Int. J. Biol. Macromol. **153**, 513 (2020)
3. R. Zhang, Q. Zeng, P. Guo, Y. Cui, Y. Sun, Environ. Sci. Pollut. Res. **27**, 16763 (2020)
4. R. Zhang, D. Li, J. Sun, Y. Cui, Y. Sun, Front. Environ. Sci. Eng. **4**, 14 (2020)
5. P.V. Sierra-Trejo, E. Guibal, F. José, J. Polym. Environ. **28**, 934 (2020)
6. Y. Xie, J. Lin, H. Lin, Y. Jiang, J. Liang, H. Wang, S. Tu, J. Li, J. Hazard. Mater. **392**, 122496 (2020)
7. H. Ouyang, N. Chen, G. Chang, X. Zhao, Y. Sun, S. Chen, H. Zhang, D. Yang, Angew. Chem. Int. Ed. **57**, 13197 (2018)
8. S. Rezania, S.M. Taib, M.F. Md Din, F.A. Dahalan, H. Kamyab, J. Hazard. Mater. **318**, 587 (2016)
9. F. Mushtaq, M.S. Sakar, M. Hoop, A.M. Lindo, X. Chen, B.J. Nelson, S. Pané, M. Guerrero, E. Pellicer, J. Sort, J. Mater. Chem. A. **3**, 23670 (2015)
10. J. Zhu, S. Wei, H. Gu, S.B. Rapole, Q. Wang, Z. Luo, N. Haldolaarachchige, D.P. Young, Z. Guo, Environ. Sci. Technol. **46**, 977 (2012)
11. X. Sun, L. Yang, Q. Li, J. Zhao, X. Li, X. Wang, H. Liu, Chem. Eng. J. **241**, 175 (2014)
12. M.T. Yagub, T.K. Sen, S. Afroze, H.M. Ang, Adv. Colloid Interface Sci. **209**, 172 (2014)
13. X. An, H. Zeng, Carbon **41**, 2889 (2003)
14. H. Sun, L. Cao, L. Lu, Nano Res. **4**, 550 (2011)
15. S.H. Huang, D.H. Chen, J. Hazard. Mater. **163**, 174 (2009)
16. Y. Li, Y. Wen, L. Wang, J. He, S.S. Al-Deyab, M. El-Newehy, J. Yu, B. Ding, J. Mater. Chem. A. **3**, 18180 (2015)

17. S. Haider, F.A.A. Ali, A. Haider, W.A. Al-Masry, Y. Al-Zeghayer, Carbohydr. Polym. **199**, 406 (2018)
18. D. Yang, L. Li, B. Chen, S. Shi, J. Nie, G. Ma, Polymer **163**, 74 (2019)
19. Y. Song, F.F. Wang, G.X. Lu, L.Y. Zhou, Q.B. Yang, J. Appl. Polym. **137**, 48279 (2020)
20. Y. Si, J. Yu, X. Tang, J. Ge, B. Ding, Nat. Commun. **5**, 5802 (2014)
21. X. Lu, C. Wang, F. Favier, N. Pinna, Adv. Energy Mater. **7**, 1601301 (2017)
22. W. Chen, S. Chen, Y. Morsi, H. El-Hamshary, M. El-Newhy, C. Fan, X. Mo, A.C.S. Appl, Mater. Interfaces **8**, 24415 (2016)
23. Chen W, Ma J, Zhu L, Morsi Y, EI-Hamshary H, Al-Deyab SS, Mo X (2016) Colloids Surfaces B Biointerfaces 142:165
24. R.M.A. Domingues, M.E. Gomes, R.L. Reis, Biomacromol **15**, 2327 (2014)
25. C. Wang, Y. Xiong, B. Fan, Q. Yao, H. Wang, C. Jin, Q. Sun, Sci. Rep. **6**, 32383 (2016)
26. Z. Qian, Z. Wang, Y. Chen, S. Tong, M. Ge, N. Zhao, J. Xu, J. Mater. Chem. A. **6**, 828 (2018)
27. Y. Si, X. Wang, C. Yan, L. Yang, J. Yu, B. Ding, Adv. Mater. **28**, 9512 (2016)
28. S. Samadi, S.S. Yazd, H. Abdoli, P. Jafari, M. Aliabadi, Int. J. Biol. Macromol. **105**, 370 (2017)
29. J. Xiao, W. Lv, Y. Song, Q. Zheng, Chem. Eng. J. **338**, 202 (2018)
30. G. Duan, M. Koehn-Serrano, A. Greiner, Macromol. Rapid Commun. **38**, 1600511 (2017)
31. G. Duan, A.R. Bagheri, S. Jiang, J. Golenser, A. Agarwal, Biomacromol **18**, 3215 (2017)
32. J. Zhao, X. Zhang, X. He, M. Xiao, W. Zhang, C. Lu, J. Mater. Chem. A **3**, 14703 (2015)
33. M. Wang, X. Li, W. Hua, L. Shen, X. Yu, X. Wang, A.C.S. Appl, Mater. Interfaces **8**, 23995 (2016)
34. S. Mousavi, F. Deuber, S. Petrozzi, L. Federer, M. Aliabadi, F. Shahraki, C. Adlhart, Colloids Surfaces A Physicochem. Eng. Asp. **547**, 117 (2018)
35. Y. Ma, B. Zhang, H. Ma, M. Yu, L. Li, J. Li, RSC Adv. **6**, 30739 (2016)
36. Y. Ma, B. Zhang, H. Ma, M. Yu, L. Li, J. Li, Sci. China Mater. **59**, 38 (2016)
37. R. Zhao, X. Li, Y. Li, Y. Li, B. Sun, N. Zhang, S. Chao, C. Wang, J. Colloid Interface Sci. **505**, 1018 (2017)
38. G. Zainab, N. Iqbal, A.A. Babar, C. Huang, X. Wang, J. Yu, B. Ding, Compos. Commun. **6**, 41 (2017)
39. J. Huang, Y. Xu, X. Zhang, Z. Lei, C. Chen, Y. Deng, C. Wang, Appl. Surf. Sci. **445**, 471 (2018)
40. X. Liang, X. Fan, R. Li, S. Li, S. Shen, D. Hu, Bioresour. Technol. **250**, 178 (2018)
41. X. Sun, L. Yang, Q. Li, Z. Liu, T. Dong, H. Liu, Chem. Eng. J. **262**, 101 (2015)
42. X. Jin, Z. Xiang, Q. Liu, Y. Chen, F. Lu, Bioresour. Technol. **244**, 844 (2017)
43. X. Jiang, Q.D. An, Z.Y. Xiao, S.R. Zhai, Z. Shi, Mater. Res. Bull. **118**, 110526 (2019)
44. S. Korpayev, C. Kavaklı, S. Tilki, P. Akkaş Kavaklı, Environ. Sci. Pollut. Res. **25**, 34610 (2018)
45. X. Li, Z. Wang, J. Ning, M. Gao, W. Jiang, Z. Zhou, G. Li, J. Environ. Manag. **217**, 305 (2018)
46. T. Wen, J. Wang, S. Yu, Z. Chen, T. Hayat, X. Wang, A.C.S. Sustain, Chem. Eng. **5**, 4371 (2017)
47. Z. Zhu, M. Zhang, W. Wang, Q. Zhou, F. Liu, Sci. Rep. **8**, 4762 (2018)
48. K. Shehzad, M. Ahmad, C. Xie, D. Zhan, W. Wang, Z. Li, W. Xu, J. Liu, J. Hazard. Mater. **373**, 75 (2019)
49. L. Lv, J. Zhang, S. Yuan, L. Huang, S. Tang, B. Liang, S.O. Pehkonen, RSC Adv. **6**, 78136 (2016)
50. S. Kobayashi, K. Hiroishi, M. Tokunoh, T. Saegusa, Macromolecules **20**, 1496 (1987)
51. C.G. Lee, P.J.J. Alvarez, A. Nam, S.J. Park, T. Do, U.S. Choi, S.H. Lee, J. Hazard Mater. **325**, 223 (2017)
52. J. Ren, S. Wang, Y. Li, Q. Yang, Y. Song, Y. Li, Chem. J. Chin. Univ. **39**, 825 (2018)